White Rose Research Online

eprints@whiterose.ac.uk
https://eprints.whiterose.ac.uk
Universities of Leeds, Sheffield and York

Deposited via The University of Sheffield.

White Rose Research Online URL for this paper:
https://eprints.whiterose.ac.uk/id/eprint/79212/

Article:
Huang, S. and Burgess, I.W. (2012) Effect of transient strain on strength of concrete and CFT columns in fire – Part 1: Elevated-temperature analysis on a Shanley-like column model. Engineering Structures, 44. 379 - 388. ISSN: 0141-0296

https://doi.org/10.1016/j.engstruct.2012.05.032

Reuse
Items deposited in White Rose Research Online are protected by copyright, with all rights reserved unless indicated otherwise. They may be downloaded and/or printed for private study, or other acts as permitted by national copyright laws. The publisher or other rights holders may allow further reproduction and re-use of the full text version. This is indicated by the licence information on the White Rose Research Online record for the item.

Takedown
If you consider content in White Rose Research Online to be in breach of UK law, please notify us by emailing eprints@whiterose.ac.uk including the URL of the record and the reason for the withdrawal request.

UNIVERSITY OF LEEDS
University of Sheffield
UNIVERSITY of York

promoting access to White Rose research papers

Universities of Leeds, Sheffield and York
http://eprints.whiterose.ac.uk/

This is an author produced version of a paper published in **Engineering Structures.**

White Rose Research Online URL for this paper:
http://eprints.whiterose.ac.uk/id/eprint/792182

Published paper
Huang, S. and Burgess, I.W. (2012) *Effect of transient strain on strength of concrete and CFT columns in fire – Part 1: Elevated-temperature analysis on a Shanley-like column model.* Engineering Structures, 44. 379 - 388. ISSN 0141-0296
http://dx.doi.org/10.1016/j.engstruct.2012.05.032

White Rose Research Online
eprints@whiterose.ac.uk

*Manuscript_v2
Click here to view linked References

10 May 2012

Effect of Transient Strain on Strength of Concrete and CFT Columns in Fire - Part1: Elevated-Temperature Analysis on a Shanley-Like Column Model

Shan-Shan Huang[a,*], Ian W. Burgess[a]

[a] Department of Civil and Structural Engineering, The University of Sheffield, Sir Frederick Mappin Building, Mappin Street, Sheffield, S1 3JD, UK

* Corresponding author. Tel.: +44 114 222 5726; Fax: +44 114 222 5793. E-mail address: s.huang@shef.ac.uk (S.-S. Huang).

Number of words: 5371 (Main text: Intro to Conclusion)
Number of figures: 13
Number of tables: 1

*Abstract

Abstract

This paper presents elevated-temperature analysis on a Shanley-like column model, as part of a study on the effect of transient strain on the strength of concrete and concrete-filled tubular columns in fire. Three high-temperature concrete material models are applied and the structural behaviours of the Shanley-like model using these three material models are compared. The effects of transient strain of concrete have been investigated by comparing the results of the analyses with and without considering this property, under the assumption that the temperature distribution within the model is uniform. The model has been evaluated against the tangent-modulus and reduced-modulus critical buckling loads at elevated temperatures. Numerical analyses have been carried out under both steady-state and transient heating scenarios, in order to investigate the influence of each on high-temperature structural analysis of the type described in this paper. It is seen that considering transient strain causes a considerable reduction of the buckling resistance, irrespective of the concrete material models and loading-heating schemes used.

Notation

A area

B model width

C_r damping coefficient of the rotational damper (Nmms)

C_v damping coefficient of the vertical damper (Ns/mm)

E Young's modulus

ε strain

$F_{s,ij}$ reaction force on spring j ($j = 1, n$ from column centre to edge) on either convex side ($i = 1$) or concave side ($i = 2$)

F_s^f spring force recorded at the end of the previous load step

F_s^{pf} spring force recorded one load step before

F_u ultimate compressive strength

F_{u0} ambient-temperature compressive strength

F_u^t tensile strength

F_{UL} spring force when unloading starts

F^* compressive force at x^*

k stiffness at linear-elastic stage

k_0 initial stiffness of the compressive curve at ambient temperature

k^* slope of the linear descending branch of the compressive curve

L model length

M_{cr} reaction moment on the rotational damper

P applied load

P_e Euler buckling load

P_t tangent-modulus critical buckling load

P_r reduced-modulus critical buckling load

P_p proportional limit

σ stress

σ_{u0} ultimate compressive stress at ambient-temperature

T temperature

t time

θ rotation

$\dot{\theta}$ velocity of θ

θ_0 initial imperfection

u vertical movement

$\dot{u}$ velocity of u

x_{ij} deformation of spring j ($j = 1, n$ from column centre to edge) on either convex side ($i = 1$) or concave side ($i = 2$)

$\dot{x}_{ij}$ velocity of x_{ij}

x_{th} thermal displacement

x_{σ} instantaneous stress-related displacement

$\dot{x}_{\sigma}$ velocity of x_{σ}

x_{σ}^{f} x_{σ} recorded at the end of the previous load step

x_{σ}^{pf} x_{σ} recorded one load step before

x_{cr} creep displacement

x_{tr} transient displacement

x_{el} elastic displacement

$x_{tr,cr}$ transient creep displacement

x_{m} mechanical displacement

x_{u} x_{σ} at the ultimate compressive strength

x_{UL} spring deformation when unloading starts

x^{*} displacement at the transition between the parabolic branch and the linear descending branch in the compression quadrant

1 Introduction

Concrete is now recognised to have a unique material property at high temperatures, defined either as transient strain (TS) or as load-induced thermal strain (LITS) [1-7]. Both of these definitions describe a phenomenon in which pre-compressed concrete, with its preload being maintained during heating, experiences a much larger compressive strain after heating than when it is loaded to the same level after being pre-heated to the same temperature. This additional strain is high in magnitude and is not recoverable, and therefore any structural analysis of a concrete structure subject to fire which neglects the transient strain property will not be able to represent the real behaviour of the structure, and will result in an incorrect prediction. Unfortunately this phenomenon is neither clearly acknowledged in the Eurocodes [8]; nor is it considered in the majority of analyses of concrete structures in fire.

Since concrete columns subjected to accidental fires are nearly always pre-compressed when they are heated, they are clearly vulnerable to the effects of transient strain. The nature of transient strain determines its significance. In stocky columns it causes considerable extra contraction across the whole cross-section, and this has been observed in many tests on short cylinders. However, as the slenderness of the columns increases, such tests become less relevant as the failure mode switches from material crushing to lateral buckling. The way in which transient strain affects buckling in such cases forms a gap in current knowledge which needs to be investigated.

A “Shanley-like” [9] column model (Fig. 1) has been established previously [10] to attempt to shed light on the mechanics of the effect of TS on buckling of heated concrete columns. Its characteristics were programmed for numerical analysis. The model was evaluated against the tangent-modulus and reduced-modulus critical buckling loads, and was found to be effective in representing the progressive change

in the regions of loading and unloading during inelastic buckling. In this paper this model is used to study the effects of transient strain of concrete on inelastic buckling at high temperatures.

There are different macroscopic mathematical models of concrete straining at high temperatures, of which the best-established are due to Anderberg and Thelandersson [1], Khoury [4, 5] and Terro [11, 12] and Schneider *et al.* [13]. The Anderberg & Thelandersson and Schneider models were developed for ordinary concretes, and there is no evidence that they are applicable to high-strength concrete, whereas the Khoury model covers nuclear-reactor-type high-strength concretes. The main distinction between these three models is their classification of the total strain into components. In this study these models, all taking into account transient strain, are applied to the Shanley-like model, to assess their differences in predicting critical loads for the simplified column. In order to isolate this effect from that of temperature distributions across the section due to different heating rates, it is assumed that the temperature distribution within the column model is uniform.

2 Steady-state heating analysis on the Shanley-like model

The Shanley-like column model is firstly analysed under steady-state heating scenario, with the mechanical loading applied at constant temperature. The aim is to find a failure load, at which overall buckling of the model occurs. In incorporating transient strain, pre-loading prior to heating is assumed, and so the analysis simulates a pre-loaded column which is heated under load to a stabilised uniform temperature; it is then unloaded and reloaded from zero at this temperature until failure occurs.

2.1 *Mathematical model & calculation procedure*

The geometry of the Shanley-like model, the fundamental formulations and solution procedure have been described in detail in a previous paper [10], and so only a brief summary of some key points will be given here. Equations (1) and (2) are derived from the equations of motion, and define the relationship between the internal and external forces and the rates of the two degrees of freedom.

$$\dot{u} = \left(P - \sum_{i=1}^{2} \sum_{j=1}^{n} F_{s,ij} \right) \Big/ C_v \tag{1}$$

$$\dot{\theta} = \left(P(\theta_0 + \theta)L - \frac{B}{2n} \sum_{j=1}^{n} j \cdot \left(F_{s,2j} - F_{s,1j} \right) \right) \Big/ C_r \tag{2}$$

The displacements of the springs are related to the two DoFs through Equations (3) and (4), on the assumption of a linear strain-gradient:

$$\left.\begin{aligned} u &= \frac{x_{1j} + x_{2j}}{2} \\ \theta &= \frac{x_{2j} - x_{1j}}{\frac{jB}{n}} \end{aligned}\right\} \quad \Rightarrow \quad \begin{cases} x_{1j} = u - \dfrac{jB}{2n}\theta \\ x_{2j} = u + \dfrac{jB}{2n}\theta \end{cases} \tag{3}$$

$$\left.\begin{aligned} \dot{u} &= \frac{\dot{x}_{1j} + \dot{x}_{2j}}{2} \\ \dot{\theta} &= \frac{\dot{x}_{2j} - \dot{x}_{1j}}{\frac{jB}{n}} \end{aligned}\right\} \quad \Rightarrow \quad \begin{cases} \dot{x}_{1j} = \dot{u} - \dfrac{jB}{2n}\dot{\theta} \\ \dot{x}_{2j} = \dot{u} + \dfrac{jB}{2n}\dot{\theta} \end{cases} \tag{4}$$

Depending on the material model used, the force-displacement relationships of the springs differ, and this affects the calculation procedure, so the applications of the three material models are described separately.

2.1.1 *Loading scheme*

The applied force is increased step by step, each load step taking a finite number of time steps. These time steps are necessary to allow the internal forces to balance

the external forces so that a new static equilibrium is reached (when the velocities $\dot{u}$ and $\dot{\theta}$ vanish and the dampers have zero force eventually); this equilibrium position is used as the initial condition for the next load step. This is repeated until the rotation of the model is seen to diverge, indicating failure by runaway buckling. In this way, the buckling load of the model at any given temperature is assessed. The whole process can be repeated at different temperatures, giving a relationship between the critical buckling loads of the model and temperature.

2.1.2 *Application of the Anderberg & Thelandersson concrete model*

The high-temperature concrete model of Anderberg and Thelandersson [1], which was derived on the basis of tests on quartzite-aggregate concrete, is applied first. For convenience in analysing the multi-spring Shanley-like model, the stress-strain relationships for equivalent solid bars are converted to force-displacement relationships by substituting Eq. (5) into the original formulations.

$$\sigma = F_s / A, \quad \varepsilon = x/L, \quad E = \frac{L}{A}k \tag{5}$$

A square bare-concrete (Grade C30) column is simulated, so the equivalent area of each spring forming part of the cross-section is $A = \frac{B^2}{2n}$. The decomposition of the total strain is converted to the following form:

$$x = x_{th} + x_{\sigma} + x_{cr} + x_{tr} \tag{6}$$

The thermal strain ε_{th} ($x_{th} = \varepsilon_{th} \cdot L$) is a simple function of temperature, which is directly given by the mean of the measured thermal strain curves in the original model. The EC2 [8] equation for thermal strain of siliceous-aggregate concrete compares reasonably well with this curve and is used in this analysis. The creep displacement x_{cr} is neglected due to its insignificance for accidental fire applications.

The relationship between the spring force F_s and the instantaneous stress-related displacement x_σ is illustrated in Fig. 2.

Rather than recording the plastic strain as in the original model, to determine the unloading route, the concurrent spring force F_{UL} and instantaneous stress-related displacement x_{UL} at the transition from loading to unloading are recorded. Linear unloading with the initial stiffness k of the compressive curve starts at Point 1, whose coordinate is (x_{UL}, F_{UL}), and ends when the tensile strength F_u^t is reached. A simplification is introduced to describe the behaviour in tension. The arrows in Fig. 2 indicate the allowed directions of loading and unloading. This simplification is justified in many cases by the fact that the tensile stresses in concrete are insignificant to the structural behaviour. In addition, the fact that the transient strain is absent in tension makes the tensile behaviour of concrete insignificant in this analysis.

The model of transient displacement for temperatures above 500°C (Eq. (8)) can not rationally be applied in a steady-state heating analysis, and so it is not used; Eq. (7) is adopted for the full temperature range.

For $20°C \le T \le 500°C$ $$x_{tr} = -k_{tr} \frac{F_s}{F_{u0}} x_{th} \tag{7}$$

For $T > 500°C$ $$\Delta x_{tr} = L \cdot \left(0.1 \times 10^{-3} \Delta T \frac{F_s}{F_{u0}} \right) \tag{8}$$

where k_{tr} is assumed to be equal to 2, which is an intermediate value taken from the range 1.8-2.35 given in the original model.

Another very important characteristic of transient strain, which needs to be accounted for, is its irrecoverability. This is done by preventing the value of the transient displacement x_{tr} from decreasing between adjacent load steps. At constant temperature the variation of x_{tr} depends solely on the spring force level, but only the spring forces at static equilibrium positions are used to account for the irrecoverability of x_{tr}. Therefore, the original model is complemented by assuming that, if the previous two load steps show a potential decrease of spring force, the value of x_{tr} is not allowed to alter from its previous value.

After all, the force-displacement relationship of the springs is defined as Eq. (9). On the basis that the displacement of each spring is the sum of three components, two of which are load-dependent, all three parts (9a, 9b and 9c) of this equation set must simultaneously be satisfied:

$$x_{tr,t} + x_{\sigma,t} = x_t - x_{th} \tag{9 a}$$

$$\begin{cases} \text{If } \; F_s^f \geq 0 \; \text{ and } \; F_s^f \geq F_s^{pf} \; \text{ then} \\ \qquad x_{tr,t} = -k_{tr} \dfrac{F_{s,t}}{F_{u0}} x_{th} \\ \text{Otherwise} \\ \qquad x_{tr,t} = x_{tr,t-\Delta t} \end{cases} \tag{9 b}$$

$$F_{s,t} = F_u \frac{x_{\sigma,t}}{x_u}\left(2 - \frac{x_{\sigma,t}}{x_u}\right) \qquad \text{Loading Stages } (N_1) \text{ and } (N_2) \tag{9 c1}$$

$$F_{s,t} = k^* x_{\sigma,t} + F^* \qquad \text{Loading Stage (D)} \tag{9 c2}$$

$$F_{s,t} = k x_{\sigma,t} + F_{UL,t} - k x_{UL,t} \qquad \text{Loading Stage (UL/RL), } F_{s,t-\Delta t} \geq F_u^t \tag{9 c3}$$

$$F_{s,t} = F_u^t \qquad \text{Loading Stage (UL/RL), } F_{s,t-\Delta t} < F_u^t \tag{9 c4}$$

where $x^* = x_u\left(1 - k^*/k\right)$, $F^* = F_u\left(1 - k^*/k\right)^2$ and $k^* = -880\dfrac{A}{L}$ (unit is MPa).

If $x_{\sigma,t-\Delta t} \geq 0$, $\dot{x}_{\sigma,t-2\Delta t} \geq 0$, $\dot{x}_{\sigma,t-\Delta t} < 0$ and $x_{\sigma,t-\Delta t} > x_{UL,t-\Delta t}$, then the transition from loading to unloading is detected:

$$\begin{aligned} F_{UL,t} &= \left(F_{s,t-2\Delta t} + F_{s,t-\Delta t}\right)/2 \\ x_{UL,t} &= \left(x_{\sigma,t-2\Delta t} + x_{\sigma,t-\Delta t}\right)/2 \end{aligned} \tag{10}$$

The calculation procedure within each time step is illustrated in Fig. 3. Relaxation with explicit time integration is used for the numerical algorithm. The two DoFs u_t and θ_t at time t are calculated from their values $u_{t-\Delta t}$ and $\theta_{t-\Delta t}$ and their velocities $\dot{u}_{t-\Delta t}$ and $\dot{\theta}_{t-\Delta t}$ at the end of the previous time step, as u and θ are assumed to increase linearly with time within each time increment. The displacement of each spring x_t at time t, and its velocity $\dot{x}_{t-\Delta t}$ at the end of the previous time step are then calculated from u_t, θ_t, $\dot{u}_{t-\Delta t}$ and $\dot{\theta}_{t-\Delta t}$ using the linear strain-gradient assumption (Equations (3) and (4)).

The loading stage (N_1), (N_2), (D) or (UL/RL) of a spring on its force-displacement curve is detected as shown in Fig. 4. This determines which of the four formulae should be used as Eq. (9 c). Unloading (Stage (UL)) is detected when the velocity $\dot{x}_{\sigma,t-\Delta t}$ of the instantaneous stress-related displacement at the end of the previous time step is negative, which indicates a decrease of the instantaneous stress-related displacement x_σ. This applies to all the time steps within one load step, except the initial one in which all the velocities are zero. In the initial time step, unloading is detected when the instantaneous stress-related displacement x_σ^f, recorded at the end of the previous load step, decreases from its value x_σ^{pf} one load step before. When unloading (UL) is detected, either Eq. (9 c3) or Eq. (9 c4) is used.

In the initial time step, when $x_{\sigma}^{f} \geq x_{\sigma}^{pf}$, or in the rest of the time steps when $\dot{x}_{\sigma,t-\Delta t} \geq 0$, loading which follows the original compressive curve (N_1), (N_2) or (D) or the linear reloading path (RL) is detected. When the instantaneous stress-related displacement $x_{\sigma,t-\Delta t}$ at the end of the previous time step is greater than or equal to $x_{UL,t}$, the original compressive curve is applied and, depending on the relationship between $x_{\sigma,t-\Delta t}$, x_u and x^* , either Eq. (9 c1) or Eq. (9 c2) is used. Otherwise, the linear reloading path of Eq. (9 c3) or Eq. (9 c4) is applied.

Solving Eq. (9), its three variables: (the transient displacement $x_{tr,t}$, the instantaneous stress-related displacement $x_{\sigma,t}$ and the concurrent spring force $F_{s,t}$) can be found. The same procedure is repeated for each of the springs. Finally, the velocities of the two DoFs $\dot{u}_t$ and $\dot{\theta}_t$ are calculated from Equations (1) and (2) for use in the next time step.

2.1.3 *Application of the Khoury & Terro concrete model*

The high-temperature concrete model given by Khoury [4] and Terro [11, 12] is also applied to the Shanley-like model. This concrete model was suggested for Portland-cement-based concretes in general, irrespective of the type of aggregate or cement blend used. An update on the strain decomposition of this concrete model has been given by Khoury [5], but no further development of the mathematical models of the strain components is introduced in this new version. Conversion of the stress-strain relationships to force-displacement relationships is again carried out, using Eq. (5). The decomposition of the total strain is converted to the following form:

$$x = x_{th} + x_{el} + x_{tr,cr} \tag{11}$$

The same model of the thermal displacement x_{th} as used for the Anderberg & Thelandersson model is applied in this section for convenience in comparing, in particular, the load-related properties of the three concrete models. Taking a typical value V_a = 65% of the aggregate content of concrete by volume, the transient creep displacement $x_{tr,cr}$ is:

$$x_{tr,cr} = L \cdot f(T) \cdot \left(0.032 + 3.226 \frac{F_s}{F_{u0}} \right) \tag{12}$$

where $f(T) = -\left(A_0 + A_1 T + A_2 T^2 + A_3 T^3 + A_4 T^4\right) \times 10^{-6}$; $A_0 = 43$, $A_1 = -2.725$, $A_2 = -6.248 \times 10^{-2}$, $A_3 = 2.193 \times 10^{-4}$ and $A_4 = -2.769 \times 10^{-7}$; $F_{u0} = \sigma_{u0} \cdot A$; C30 concrete is used, so σ_{u0} = 30MPa.

The irrecoverability of $x_{tr,cr}$ is treated in similar fashion to the irrecoverability of x_{tr} as formulated in Eq. (9b). Due to the simplifications introduced by Khoury & Terro, a relationship between the spring force F_s and the <u>total</u> spring displacement x, as formulated in Eq. (13), can be achieved.

For loading stage (L), if $F_s^f \geq 0$ and $F_s^f \geq F_s^{pf}$: (13 a)

$$F_{s,t} = \left(x_t - x_{th} - 0.032 L \cdot f(T)\right) \Big/ \left(\frac{3.226 L \cdot f(T)}{F_{u0}} + \frac{1}{k_0} \right)$$

Otherwise at loading stage (L): (13 b)

$$F_{s,t} = k_0 \left(x_t - x_{tr,cr,t-\Delta t} - x_{th} \right)$$

For loading stage (UL/RL), if $F_{s,t-\Delta t} \geq F_u^t$: (13 c)

$$F_{s,t} = k x_t + F_{UL,t} - k x_{UL,t}$$

For loading stage (UL/RL), if $F_{s,t-\Delta t} < F_u^t$: (13 d)

$$F_{s,t} = F_u^t$$

In terms of unloading and possible reloading (UL/RL), the reference point (x_{UL}, F_{UL}) should be taken from the full force-displacement (F_s - x) curve, and unloading should be detected on the basis of the total spring displacement x and its velocity $\dot{x}$, rather

than the instantaneous stress-related displacement x_σ and its velocity $\dot{x}_\sigma$, as in the previous section. Therefore, the transition from loading to unloading is detected if $x_{t-\Delta t} \geq x_{th} + 0.032L \cdot f(T)$, $\dot{x}_{t-2\Delta t} \geq 0$, $\dot{x}_{t-\Delta t} < 0$ and $x_{t-\Delta t} > x_{UL,t-\Delta t}$.

The corresponding spring force F_{UL} and displacement x_{UL} are calculated as:

$$\begin{aligned} F_{UL,t} &= \left(F_{s,t-2\Delta t} + F_{s,t-\Delta t}\right)/2 \\ x_{UL,t} &= \left(x_{t-2\Delta t} + x_{t-\Delta t}\right)/2 \end{aligned} \tag{14}$$

The initial value of the spring displacement x_0 and the initial value of the displacement $x_{UL,0}$ at this transition are both equal to $x_{th} + 0.032L \cdot f(T)$, given by Eq. (13 a) when $F_s = 0$.

Another important issue is that, although the full force-displacement (F_s - x) curve is used, the stiffness of the linear unloading path should still be the initial stiffness k of the curve of force against instantaneous stress-related displacement (F_s - x_σ), because none of the spring displacement components except the elastic displacement x_{el} is recoverable. Using the initial stiffness of the F_s - x curve would lead to an erroneous prediction of the spring displacement, especially for its irrecoverable components. The relationship between σ and ε_σ was not measured in the experiments carried out by Khoury [2, 3], although a model was given by Khoury [4] on the basis of Schneider's [6] test results. Therefore, for simplification, the initial stiffness k of the F_s - x_σ curve is derived from the Young's modulus E of the Schneider model, which is related to the load-history factor $\alpha = \dfrac{\sigma_{history}}{\sigma_{u0}}$. The literature lacks a clear definition of $\sigma_{history}$, and so α is simplified and converted to

$\alpha = \frac{F_s^f}{F_{u0}}$. The original model only gives the formulation of E for α = 0, α = 0.1 and $\alpha \geq$ 0.3, and so it is assumed that linear interpolation determines E for intermediate values of α.

The general calculation procedure is the same as that for the Anderberg & Thelandersson model. The only differences are that Eq. (13) is used to replace Eq. (9) and that the spring force F_s is directly calculated from the concurrent spring displacement x. Fig. 5 shows the process for detection of the loading stage, which is also similar to that used in the previous section, except that it is done on the basis of the total spring displacement x and velocity $\dot{x}$, and that there are only three loading stages.

2.1.4 *Application of the Schneider concrete model*

The application of the concrete model given by Schneider *et al.* [13] is described in this section. This model was developed for three types (quartzite, limestone and lightweight) of structural concretes. Eq. (5) is again used to convert the stress-strain relationships to force-displacement relationships. The decomposition of the total strain becomes:

$$x = x_{th} + x_m \tag{15}$$

The same model of thermal displacement x_{th} used in the previous two sections is again applied in this section. The mechanical displacement x_m is given by:

$$x_m = \frac{F_s}{k}(1 + \varphi) \tag{16}$$

where φ is solely related to temperature for any given type of concrete. Its value for quartzite concrete is used, for convenience in comparing the three models,

since the Anderberg & Thelandersson model is based solely on tests on quartzite-aggregate concrete. A suggested value of moisture content w = 2% is adopted [7].

Although the recoverable elastic displacement x_{el} is included in the mechanical displacement x_m, since the magnitude of x_{el} is very small the irrecoverability of x_m is accounted for in the same way as described in the previous two sections. As in applying the Khoury & Terro model, this force-displacement relationship is also a full constitutive relationship between the spring force F_s and total spring displacement x:

For loading stage (L), if $F_s^f \geq 0$ and $F_s^f \geq F_s^{pf}$:

$$F_{s,t} = \frac{k\left(x_t - x_{th}\right)}{1+\varphi} \tag{17 a}$$

Otherwise at loading stage (L):

$$F_{s,t} = F_{s,t-\Delta t} \tag{17 b}$$

For loading stage (UL/RL), if $F_{s,t-\Delta t} \geq F_u^t$:

$$F_{s,t} = kx_t + F_{UL,t} - kx_{UL,t} \tag{17 c}$$

For loading stage (UL/RL), if $F_{s,t-\Delta t} < F_u^t$:

$$F_{s,t} = F_u^t \tag{17 d}$$

Therefore, the loading stage is again detected on the basis of x and its velocity $\dot{x}$ and hence the transition from loading to unloading is detected, if $x_{t-\Delta t} \geq x_{th}$, $\dot{x}_{t-2\Delta t} \geq 0$, $\dot{x}_{t-\Delta t} < 0$ and $x_{t-\Delta t} > x_{UL,t-\Delta t}$. The concurrent spring force and displacement are calculated as:

$$\begin{aligned} F_{UL,t} &= \left(F_{s,t-2\Delta t} + F_{s,t-\Delta t}\right)/2 \\ x_{UL,t} &= \left(x_{t-2\Delta t} + x_{t-\Delta t}\right)/2 \end{aligned} \tag{18}$$

The initial value of the spring displacement x_0 and the initial value of the displacement $x_{UL,0}$ at this transition are both equal to x_{th}. The stiffness of the linear unloading path should still be the initial stiffness k of the F_s-x_σ curve. The definition

of k has been described in detail in the previous section. The general calculation procedure is the same as that for the previous two models, except that Eq. (17) is used to calculate the spring force $F_{s,t}$ on the basis of the concurrent spring displacement x_t. The loading stage, determining which of the four formulae in Eq. (17) should be used, is detected in the same way as described in the previous section, as shown in Fig. 5.

2.2 *Behaviour of the Shanley-like column model under steady-state uniform heating*

2.2.1 *Results of analysis using the Anderberg & Thelandersson model*

An example model was created, whose dimensions were chosen to ensure that the failure mode of the model at any given temperature is overall buckling in the inelastic range. The specification of the model is given in Table 1. A model with only four springs (two on each side) is adopted for convenience in understanding the analytical results at elevated temperatures. A convergence test was done on the size of the time increment t. Due to the nature of the calculation procedure itself this analysis is quite independent from the size of Δt as long as it is fine enough for the numerical process to proceed. When an oversized Δt is applied a numerical instability ensues, but otherwise very little difference is made to the results by varying Δt.

Figures 6 and 7 plot selected structural responses of the model at 500°C. The results of the analysis are divided into two groups, one including the transient straining of concrete and one without, in order to investigate its influence on the mechanics of inelastic buckling at high temperature. Fig. 6 shows the total spring displacement and its three components, for the two springs at the edges of the model, throughout the time steps of the successive load steps. The force-displacement

relationships $F_{s,ij} - x_{\sigma,ij}$ of both the outer and inner springs during the same period are plotted in Fig. 7.

Some of the springs on the convex side start to unload when the applied force and its consequent rotation are sufficiently large. This results in differential instantaneous stress-related displacement $x_{\sigma,ij}$ and differential transient displacement $x_{tr,ij}$ among the springs, because these are both load-related. This naturally causes differential total spring displacement x_{ij} among the springs, as illustrated in Fig. 6. At failure, the difference in displacement between the concave- and convex-side springs diverges.

The inclusion of transient strain causes the buckling load of the model to decrease significantly compared with the case when the transient displacement is set to zero. This corresponds to the much lower spring-load levels and much smaller $x_{\sigma,ij}$ shown in the 'TS' parts of Figures 6 and 7 than those shown in the 'no TS' parts. Fig. 7 shows that without considering TS the force-displacement relationships of the springs show evident nonlinearity, long before failure occurs, whilst with the involvement of TS the spring forces are so low that the spring force-displacement curves still appear to be linear. Although, when TS is included, the displacements $x_{\sigma,ij}$ are much smaller than when there is no TS, the total spring displacements x_{ij} and the two DoFs u and θ have magnitudes very similar to those resulting when TS is excluded, because they are complemented by the transient displacement $x_{tr,ij}$. This may explain the much lower buckling load when x_{tr} is taken into account.

Plotting, at various temperatures, the ultimate buckling loads of the model, with and without considering TS, together with the idealised critical buckling loads P_e, P_r and P_t and the proportional limit P_p, gives Fig. 8. Without including TS, the buckling

load of the model at an arbitrary temperature lies between P_t and P_r at the same temperature. This is consistent with the statement in Shanley's theory [9] that the tangent- and reduced-modulus critical buckling loads are the lower and upper bounds of the inelastic buckling loads, if P_t and P_r are calculated on the basis of the force-displacement (F_s - x_σ) relationship given by Fig. 2, which does not include TS. The critical buckling loads are closer to P_t than to P_r, which results from the decreasing tangent modulus of the nonlinear force-displacement curve. A similar phenomenon is also described by Shanley for structural materials with reducing tangent moduli.

The indication from the Shanley-like column model is that the involvement of TS (at least for the Anderberg & Thelandersson concrete model) may cause a large reduction of the buckling resistance of an intermediate-length concrete column at elevated temperatures. This result is revealing, because the effects of TS on the buckling of concrete columns are usually ignored in structural fire modelling, which may lead to unsafe prediction of the capacities of such elements. This is less surprising if the stress-dependence of TS is considered. The study of the mechanics of inelastic buckling, an example of which (at 500°C) is described above, indicates that, when a column starts to bend, the bending causes differential stresses between its concave and convex faces. At elevated temperatures this difference between the compressive stresses will cause differential TS, which will cause a further difference of the strains between the two sides, leading to further bending. Due to the rather large magnitude of TS this iterative effect will be significant, and actually causes the column to lose stability at a much lower load than when TS is absent.

2.2.2 *Model comparisons*

The high-temperature concrete models given by Khoury & Terro and Schneider were also implemented in the same four-spring model used with the Anderberg &

Thelandersson concrete model. Since the decomposition of the total strain is different in each of these models, it is not possible to compare each strain component individually, and so the comparisons shown in this section are all based on total strain.

Fig. 9 shows the buckling loads of the multi-spring model over a range of temperatures, applying the three high-temperature concrete models. It should be noted that the buckling loads have been nominalised against the critical buckling load at room temperature when using the Anderberg & Thelandersson (A&T) model. This figure also plots the high-temperature strength reduction factors for normal-weight concrete given by Eurocode 2 [8], which tracks the results given by adopting the A&T model without TS in the high-temperature and low-temperature regions. It is shown that the two curves resulting from the A&T and Khoury & Terro (K&T) models are very close to each other over the whole temperature range, whilst the curve from the Schneider model is quite separate from them, except that it almost converges with them at temperatures above 600°C. Below this range, the A&T and K&T models lead to lower predictions of buckling resistance than Schneider. The A&T model, which has the most refined strain decomposition among the three models, proved suitable for use in the rest of this research.

Although the strain definitions and formulations of these three models are completely different, they all show a reduction of buckling resistance due to the involvement of transient strain, at least for the majority of the temperature range, compared with the case in which A&T is applied without the TS component.

3 Transient heating scenario

When structures are subject to accidental fires they are usually already carrying in-service loading. In multi-storey frames the columns in particular continue to carry these pre-loads throughout the fire, although the forces in the elements of flooring

systems may change radically due to thermo-mechanical effects. Therefore, especially for columns, it is more rational to seek a failure temperature at constant load than to seek a failure load at constant temperature. At least these two approaches should be compared, in order to decide whether it is necessary to involve the complexity inherent in transient heating. Therefore, the transient heating scenario is also modelled with the Shanley-like model.

3.1 *Mathematical model & calculation procedure*

3.1.1 *Loading scheme*

The loading-heating process is more complex than that used in the steady-state heating approach. The imposed load is firstly applied in steps at ambient temperature. Then, maintaining the load constant, the transient heating is applied step-by-step, similar to the application of step loading. In this way, the buckling temperature of the model at any given load level is assessed. Repeating this procedure for various load levels, a relationship between the buckling temperature of the model and the applied load level is found. It should also be noted that the assumption that the temperature distribution within the multi-spring model is uniform is still applied in this analysis, although it would be unrealistic in a solid cross-section.

3.1.2 *Application of the Anderberg & Thelandersson concrete model*

When applying the step loading at ambient temperature, the calculation procedure within each load step is exactly the same as in the steady-state heating approach. For further application of the heating steps, the same mathematical model is still adopted, except that the full formula (both Eq. (7) and Eq. (8)) of the transient strain ε_{tr} may be used under this transient heating condition, and so Eq. (9b) is replaced by:

$$
\begin{cases}
\text{If } F_s^f \geq 0 \text{ and } F_s^f \geq F_s^{pf} \text{ then} & \\
\quad x_{tr,t} = -k_{tr} \dfrac{F_{s,t}}{F_{u0}} x_{th} & \left(20°\text{C} \leq T \leq 500°\text{C}\right) \\
\quad x_{tr,t} = x_{tr,t-\Delta t} + L \cdot \left(0.1 \times 10^{-3} \Delta T \dfrac{F_{s,t}}{F_{u0}} \right) & \left(T > 500°\text{C}\right) \\
\text{Otherwise} & \\
\quad x_{tr,t} = x_{tr,t-\Delta t} &
\end{cases} \tag{19}
$$

Fig. 10 shows the process for discrimination between loading and unloading. While applying load at ambient temperature, it is the same as in the steady-state heating analysis. For further heating steps, it remains the same, except during the initial time step at each temperature. In this time step, unloading is assumed not to take place, and the change of the force-displacement relationship with temperature is accounted for by the spring displacement x_σ remaining the same as at the end of the previous temperature step. The spring force F_s at this unchanged x_σ is then re-calculated according to the updated force-displacement relationship.

3.2 *Effects of transient heating on the behaviour of the Shanley-like column model*

The four-spring model used in the steady-state heating analysis has been re-evaluated for the transient heating scenario. The structural response of the model subject first to step loading and then to step heating is shown below, up to the critical temperature beyond which overall buckling of the model occurs. A typical load ratio LR = 0.6 (imposed force = 60% of the buckling load of the model at room temperature), is applied. The results of the analysis are again divided into two groups, depending on whether transient strain of concrete is taken into account. In the figures, the labels 'TS' and 'No TS' are again used to distinguish these two groups of results. Fig. 11 shows the displacements of the two outer springs

throughout the time steps during which loading and then temperature increase occur. The force-displacement relationship $F_{s,ij}^{f} - x_{\sigma,ij}^{f}$ of each spring at the end of each load/temperature step during the same period is plotted in Fig. 12.

For all the load/temperature steps except the last one, the spring displacements are always initiated in the first time step at each load or temperature, and then re-stabilise after a certain period of time, as shown in Fig. 11. Without considering transient strain, a sudden increase of T and sudden decreases of $x_{th,ij}$ and x_{ij} in the initial range (at temperatures from 20°C to 100 °C) are observed. This results from the rapid re-stabilisation of the motion in each temperature step, since the force-displacement ($F_s - x_\sigma$) curves of the springs do not alter within this temperature range. Alteration of the thermal displacement $x_{th,ij}$ with temperature will not cause any additional $F_{s,ij}$ because $x_{th,ij}$ is not load-related. This phenomenon does not take place when TS is included, because the alteration of the transient displacement $x_{tr,ij}$ with temperature rise causes an additional $F_{s,ij}$ due to the load-dependence of $x_{tr,ij}$.

The differential displacements across the springs, illustrated in Fig. 11, result from the unloading of some of the convex-side springs, shown in Fig. 12. At failure, the difference of the spring displacements between the concave and convex sides diverges, which corresponds to a divergence of the model's rotation. It should be noted that the spring displacements and forces, after significant divergence of the rotation of the model has occurred, are excluded in the 'TS' parts of Figures 11 and 12, in order to show their development before failure more clearly. The transient displacements $x_{tr,ij}$ of the unloading springs do not decrease when both their $x_{\sigma,ij}$ and x_{ij} decrease as the spring forces decrease. This is because the decrease of

$x_{tr,ij}$ between adjacent load/temperature steps is prevented in the numerical modelling, in order to account for the irrecoverability of TS.

Including transient strain in the analysis causes the critical temperature, at which buckling of the model occurs, to decrease significantly from that when TS is not taken into account. This results in much lower absolute values of thermal displacements $x_{th,ij}$ in the 'TS' part of Fig. 11 than those in the 'no TS' part of this figure. In Fig. 12, the initial simultaneous gradients of the force-displacement curves are approximately linear, and are identical in both the 'No TS' and 'TS' cases. They result from the step loading at room temperature, which does not induce significant rotation of the model. After a heating step is imposed, without TS, the degradation of the material with temperature rise causes $x_{\sigma,ij}$ to increase under almost unchanged $F_{s,ij}$, until buckling occurs. However, the involvement of TS causes a considerable amount of rotation of the model, and evident differences of the spring forces and rotations happen at much lower temperatures than when TS is excluded. The spring force-displacement curves are still approximately linear just before failure occurs, as seen in the 'TS' part of Fig.12.

Plotting, for a range of load levels (nominalised against the critical buckling load at 20°C when using the A&T model), the ultimate buckling temperatures of the models with and without TS, on the curves of Fig. 9, gives Fig. 13. In this figure, the circles and triangles illustrate the results of the analysis in which a transient heating scenario is applied. Comparing these with the results of the steady-state heating analysis shows that there is very little difference between these two heating scenarios, suggesting that the steady-state heating approach is adequate when a uniform temperature distribution within the model is assumed. However, the influence of the heating scenario is expected to be more significant if a thermal gradient exists across the springs. In particular, the magnitude of the additional spring forces and

displacements caused by the thermal gradients could be significantly affected by the loading and heating histories. Therefore, in further analyses in which non-uniform temperature distributions through column cross-sections are represented, the transient heating approach should be applied for a better prediction of the spring forces and displacements on the basis of a more realistic loading-heating history. It should also be noted that the use of the complementary formula for x_{tr} (Eq. (8)) using Anderberg & Thelanderssons' concrete model for temperatures above 500°C leads to a lower prediction of the buckling resistance, and so the predicted buckling resistances based on the three material models are approximately the same beyond 600 °C.

4 Conclusions

Irrespective of the concrete material models and loading-heating schemes used, considering transient strain causes a considerable reduction of the buckling resistance of the model. This suggests that ignoring the effects of TS on the buckling of concrete columns in structural modelling may lead to unsafe predictions of the capacities of such elements. The reduction of the buckling resistance due to the inclusion of TS is induced by an interactive process in which the bending of the column causes differential stresses between its concave and convex sides, and in turn causes differential TS. This causes a further difference of strains between the two sides, leading to further bending. This interactive effect is very significant, due to the large magnitude and irrecoverability of TS. It actually causes the column to lose stability at much lower load/temperature levels in both the steady-state and transient heating analyses, than when TS is absent.

The comparison of the three concrete models in the steady-state heating analysis indicates that the A&T and K&T material models give very close predictions of the failure loads of the model at constant temperature, whilst the Schneider material

model results in a considerably higher prediction of critical load than the other two, at temperatures below 600°C. Compared with the case in which the Anderberg & Thelandersson model is applied without TS, all three models show a reduction of the buckling resistance due to the involvement of transient strain.

There is very little difference between the steady-state and transient heating scenarios when a uniform temperature distribution is assumed. However, when non-uniform temperature distributions through column cross-sections are simulated, the transient heating approach is suggested for a more precise evaluation of the spring forces and displacements, on the basis of a more realistic loading-heating history.

ACKNOWLEDGMENT: *The principal author is grateful for the support of Corus Group Ltd and the Engineering and Physical Sciences Research Council of the United Kingdom, under a Dorothy Hodgkin Postgraduate Award.*

References

[1] Anderberg Y, Thelanderson S. Stress and deformation characteristics of concrete at high temperatures. 2. Experimental investigation and material behaviour model. Bulletin 54. Sweden: Lund University; 1976.

[2] Khoury GA, Grainger BN, Sullivan PJE. Transient thermal strain of concrete: literature review, conditions within specimen and behaviour of individual constituents. Mag Concrete Res 1985; 37(132):131-44.

[3] Khoury GA, Grainger BN, Sullivan PJE. Strain of concrete during first heating to 600°C under load. Mag Concrete Res 1985; 37(133):195-215.

[4] Khoury GA. Performance of heated concrete - Mechanical properties. Contract NUC/56/3604A with Nuclear Installations Inspectorate of the Health and Safety Executive. London: Imperial College; 1996.

[5] Khoury GA. Strain of heated concrete during two thermal cycles. Part 1: Strain over two cycles, during first heating and at subsequent constant temperature. Mag Concrete Res 2006; 58(6):367-85.

[6] Schneider U. Properties of materials at high temperatures - Concrete. RILEM 44-PHT. Kassel: University of Kassel; 1985.

[7] Schneider U, Horvath J. Behaviour of ordinary concrete at high temperatures. Research Report Vol. 9. Vienna: Institute of Building Materials, Building Physics and Fire Protection, Vienna University of Technology; 2003.

[8] European Committee for Standardization (CEN). BS EN 1992: Eurocode 2: Design of concrete structures - Part 1-2: General rules - Structural fire design. Brussels: CEN; 2004.

[9] Shanley FR. Inelastic column theory. J Aero Sci 1947; 14(5):261-8.

[10] Huang S-S, Burgess I, Huang Z, Plank R. The mechanics of inelastic buckling using a Shanley-like model. P I Civil Eng-Eng Comp Mech 2011; 164(2):103-19.

[11] Terro MJ. Computer modelling of the effect of fire on structures. Ph.D. thesis. London: Department of Civil Engineering, Imperial College of Science and Technology, London University; 1991.

[12] Terro MJ. Numerical modelling of the behaviour of concrete structures. ACI Struct J 1998; 95(2):183–93.

[13] Schneider U, Schneider M, Franssen J-M. Consideration of nonlinear creep strain of siliceous concrete on calculation of mechanical strain under transient temperatures as a function of load history. In: Proceedings of the 5th international conference – structures in fire. 2008. p. 463-76.

Figure Captions

Figure 1 Shanley-like column model.

Figure 2 The relationship between the spring force and the instantaneous stress-related displacement based on the Anderberg & Thelandersson model.

Figure 3 Calculation procedure within each time step of the steady-state heating analysis using the Anderberg & Thelandersson concrete model.

Figure 4 Detection of loading stage when Anderberg & Thelandersson concrete model and steady-state heating scenario are applied.

Figure 5 Detection of loading stage when Khoury & Terro concrete model is applied.

Figure 6 Development of the total spring displacement and its three components over time, with and without the consideration of transient straining.

Figure 7 Compressive force-displacement curves of the springs under the steady-state heating scenario.

Figure 8 Buckling loads of the model with and without TS, compared with theoretical buckling loads and proportional limits at elevated temperatures.

Figure 9 Comparison of various high-temperature concrete material models involving TS on the buckling resistance of the multi-spring model.

Figure 10 Detection of the loading stage when the Anderberg & Thelandersson concrete model and transient heating scenario are applied.

Figure 11 Development of the total spring displacement and its three components under step loading followed by step heating.

Figure 12 Compressive force-displacement curves of the springs under the transient heating scenario.

Figure 13 Comparison between the steady-state and transient heating scenarios on the buckling resistance of the multi-spring model.

Table Captions

Table 1 Specification of the example model analysed.

Table 1

L (mm)	B (mm)	n	θ_0 (rad)	C_v (Ns/mm)	C_r (Nmms)	Δt (s)	ΔP (N)
150	15	2	1E-12	2000	2000	1E-4	100

Table 1 Specification of the example model analysed.

Figure 1

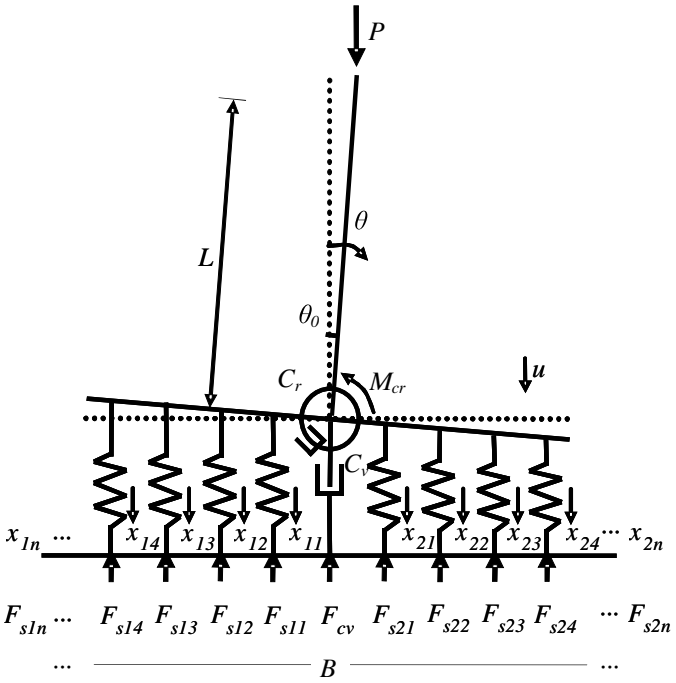

Figure 1 Shanley-like column model.

Figure 2

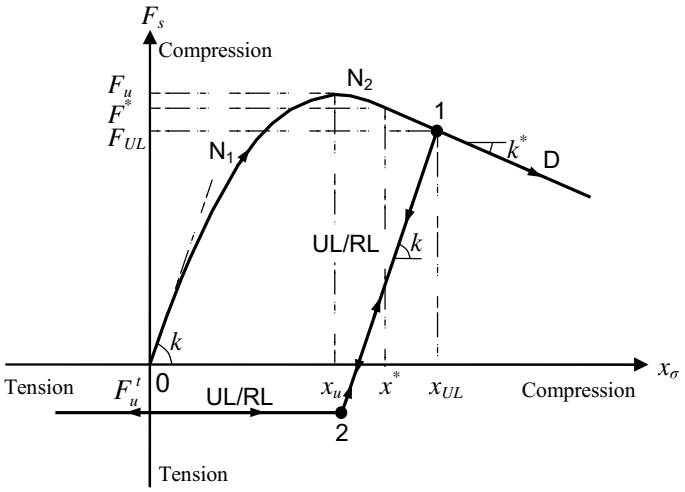

Figure 2 The relationship between the spring force and the instantaneous stress-related displacement based on the Anderberg & Thelandersson model.

Figure 3

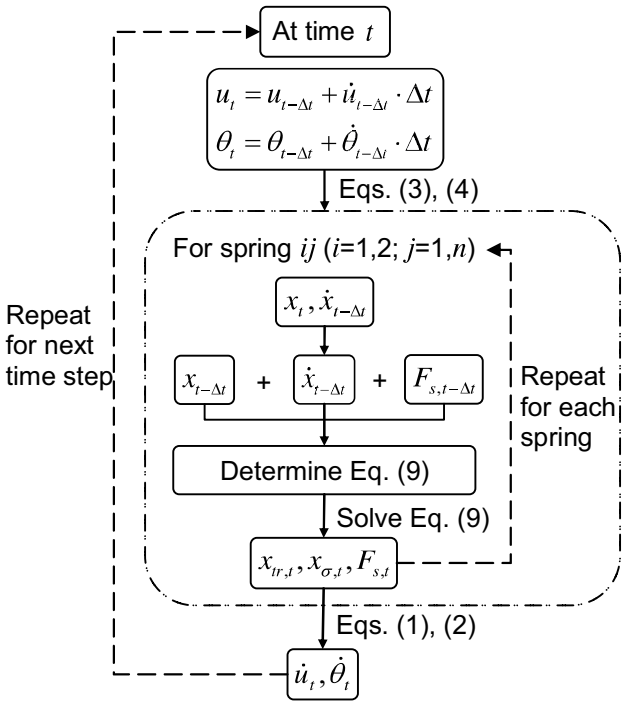

Figure 3 Calculation procedure within each time step of the steady-state heating analysis using the Anderberg & Thelandersson concrete model.

Figure 4

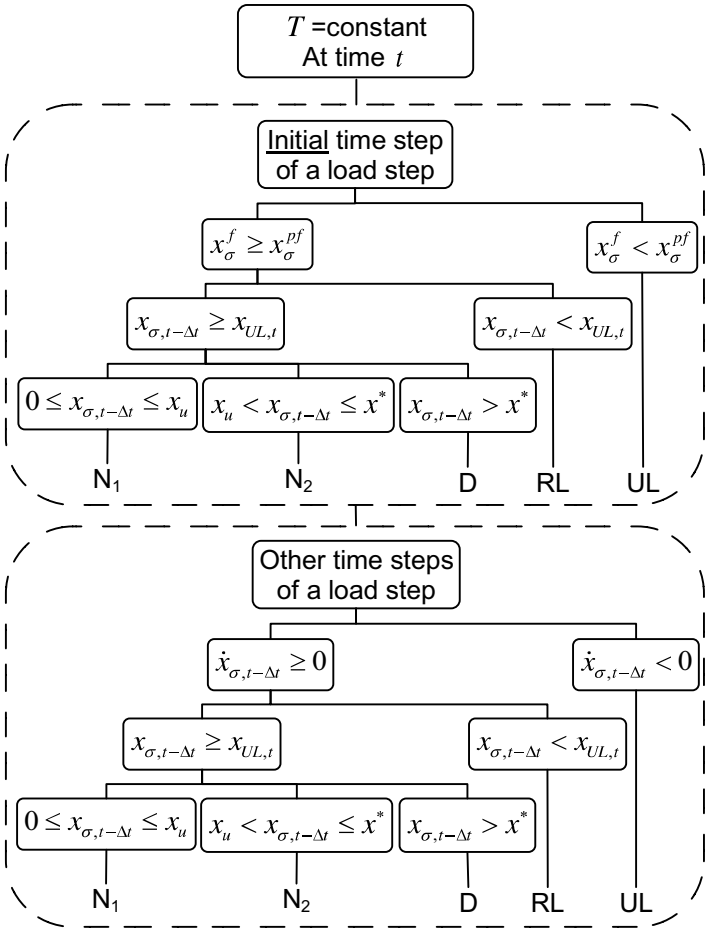

Figure 4 Detection of loading stage when Anderberg & Thelandersson concrete model and steady-state heating scenario are applied.

Figure 5

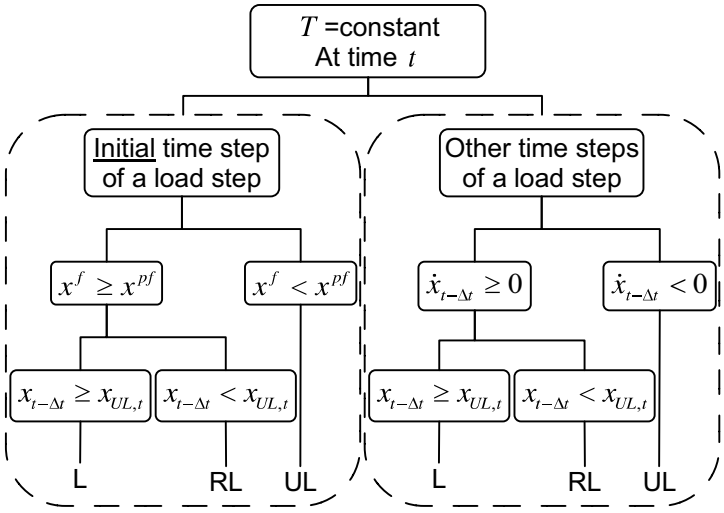

Figure 5 Detection of loading stage when Khoury & Terro concrete model is applied.

Figure 6

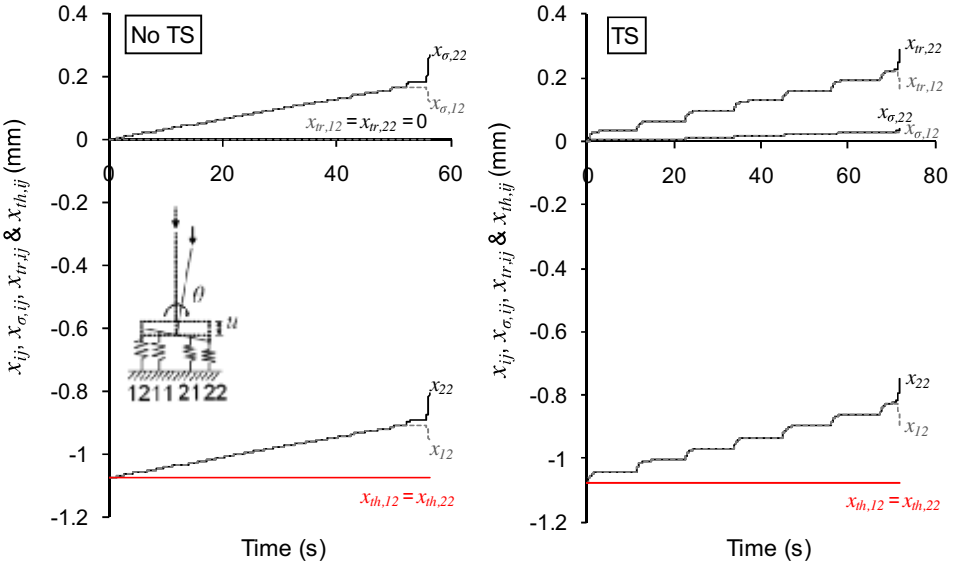

Figure 6 Development of the total spring displacement and its three components over time, with and without the consideration of transient straining.

Figure 7

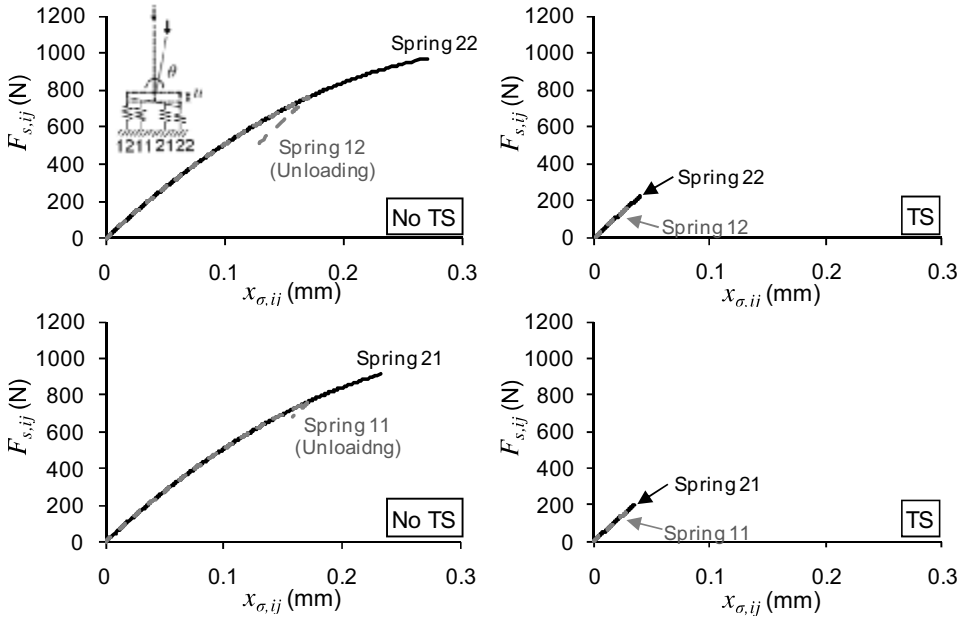

Figure 7 Compressive force-displacement curves of the springs under the steady-state heating scenario.

Figure 8

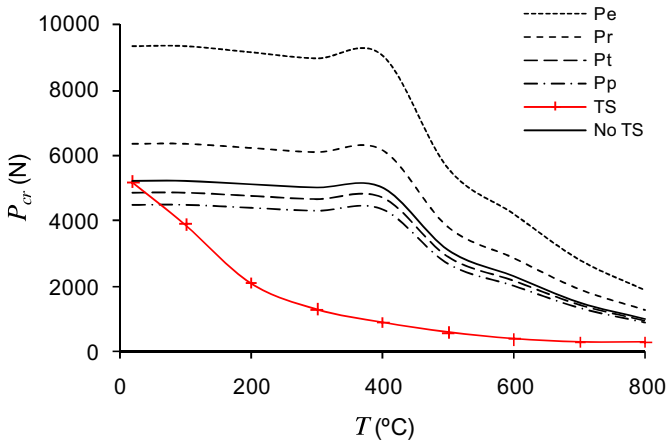

Figure 8 Buckling loads of the model with and without TS, compared with theoretical buckling loads and proportional limits at elevated temperatures.

Figure 9_v2

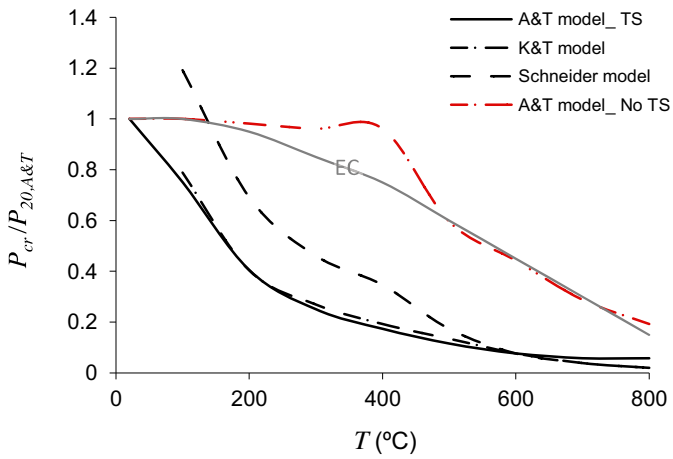

Figure 9 Comparison of various high-temperature concrete material models involving TS on the buckling resistance of the multi-spring model.

Figure 10

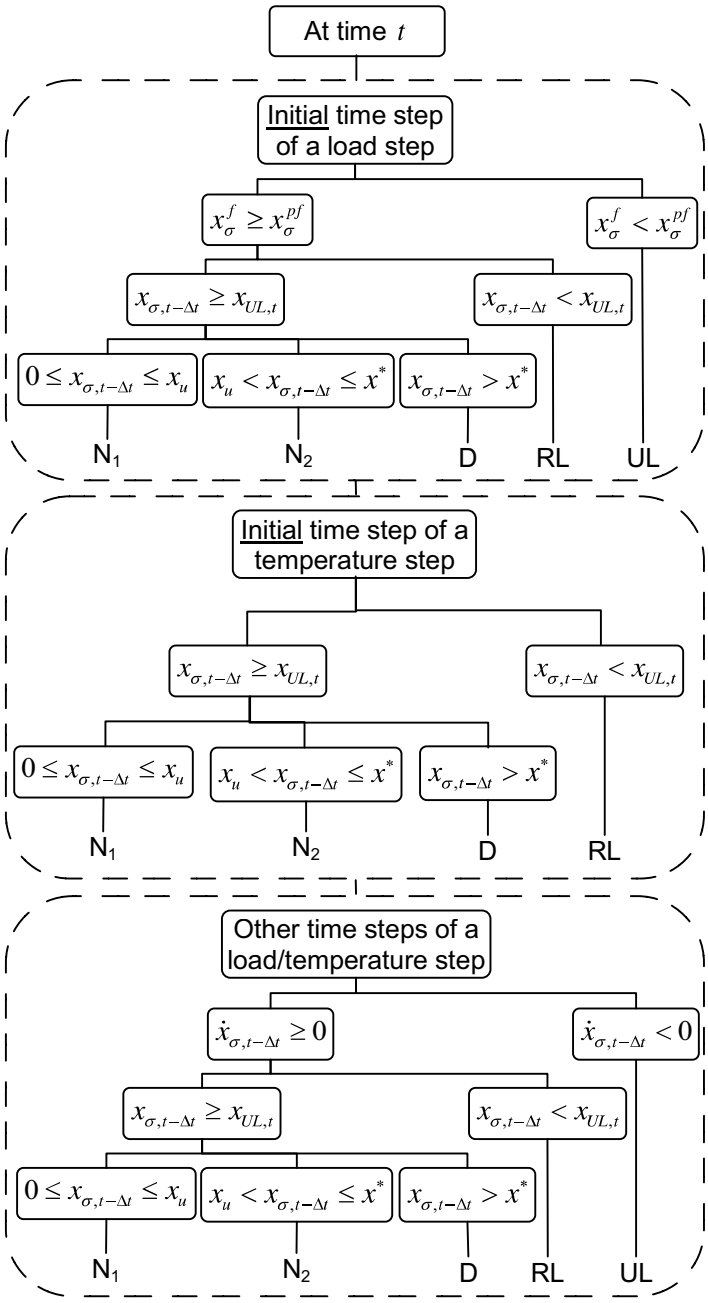

Figure 10 Detection of the loading stage when the Anderberg & Thelandersson concrete model and transient heating scenario are applied.

Figure 11

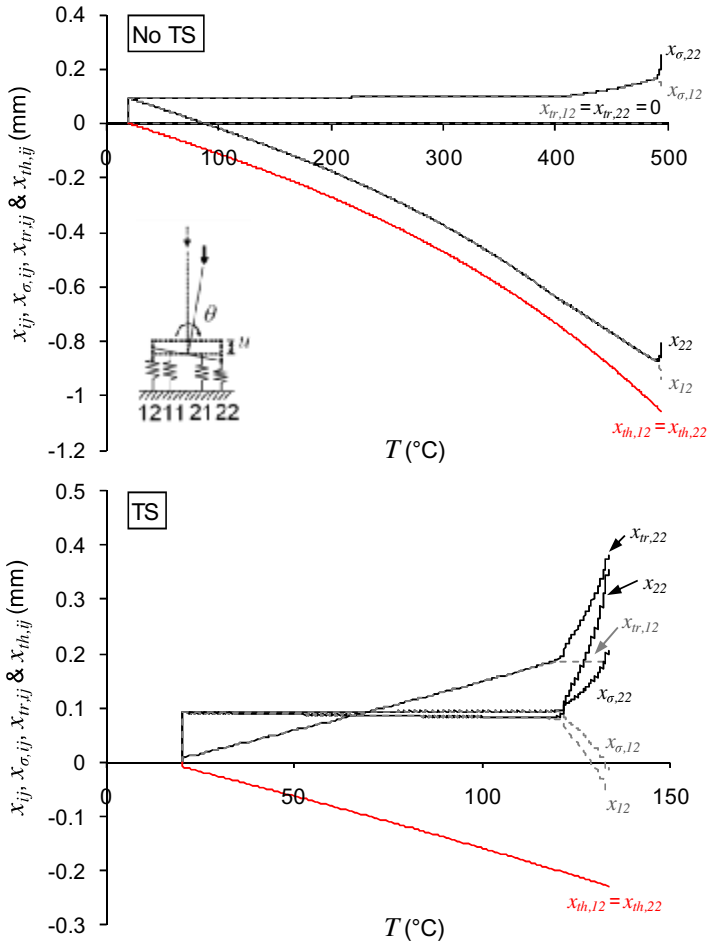

Figure 11 Development of the total spring displacement and its three components under step loading followed by step heating.

Figure 12

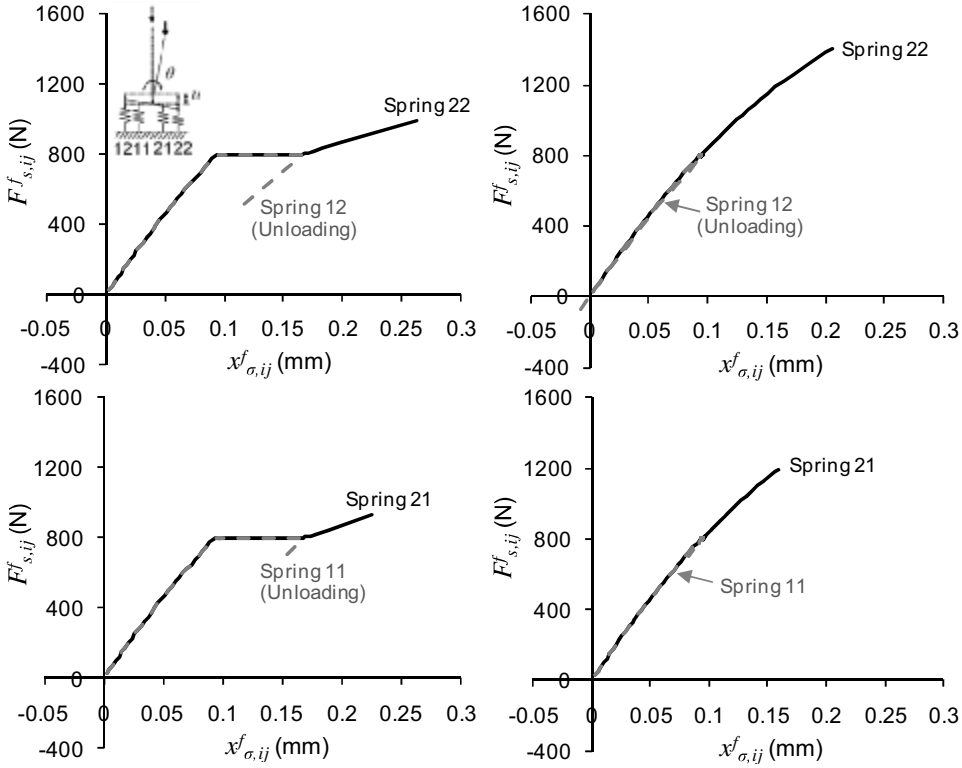

Figure 12 Compressive force-displacement curves of the springs under the transient heating scenario.

Figure 13_v2

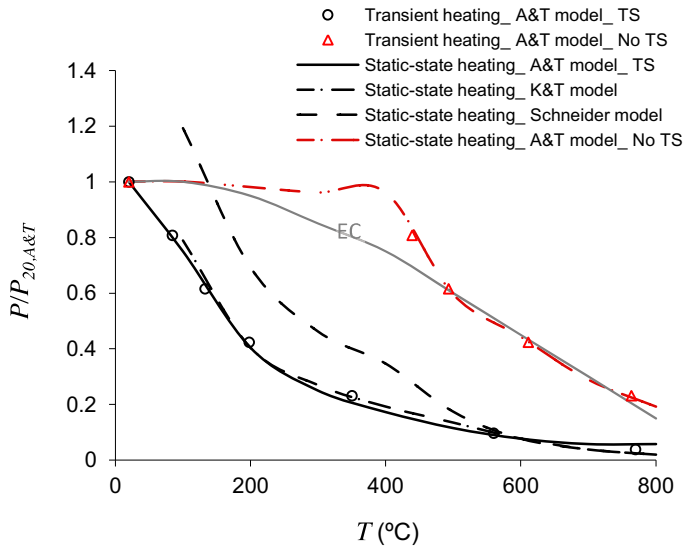

Figure 13 Comparison between the steady-state and transient heating scenarios on the buckling resistance of the multi-spring model.